HAMAMATSU PRESENTS

ANALYTICAL TALKS

WATCH NOW ▶

Taming Ultrafast Laser Filaments for Optimized Semiconductor–Metal Welding

Maxime Chambonneau,* Qingfeng Li, Vladimir Yu. Fedorov, Markus Blothe, Kay Schaarschmidt, Martin Lorenz, Stelios Tzortzakis, and Stefan Nolte

Ultrafast laser welding is a fast, clean, and contactless technique for joining a broad range of materials. Nevertheless, this technique cannot be applied for bonding semiconductors and metals. By investigating the nonlinear propagation of picosecond laser pulses in silicon, it is elucidated how the evolution of filaments during propagation prevents the energy deposition at the semiconductor–metal interface. While the restrictions imposed by nonlinear propagation effects in semiconductors usually inhibit countless applications, the possibility to perform semiconductor–metal ultrafast laser welding is demonstrated. This technique relies on the determination and the precompensation of the nonlinear focal shift for relocating filaments and thus optimizing the energy deposition at the interface between the materials. The resulting welds show remarkable shear joining strengths (up to 2.2 MPa) compatible with applications in microelectronics. Material analyses shed light on the physical mechanisms involved during the interaction.

1. Introduction

The technological revolution provided by ultrafast lasers originates from the remarkable degree of control offered by femtosecond pulses on the energy deposition occurring prior to the material response after a few picoseconds.[1–4] While ultrashort laser pulses represent an extraordinary tool for clean material removal with applications in material processing[5] or nanosurgery,[6] they are also attractive for additive manufacturing as they offer the possibility of joining a wide variety of materials that are impossible to bond using standard welding procedures. Nowadays, ultrafast laser welding can be successfully applied in configurations such as glass–metal,[7] glass–semiconductor,[8] glass–glass,[9,10] polymer–polymer,[11] and, more recently, ceramic–ceramic,[12] yielding MPa shear joining strengths. Given that this order of magnitude is similar or even higher than the one that can be obtained with traditional bonding methods (e.g., adhesive bonding), laser welding is an attractive alternative to these as it shows no aging or degasification problem. Nevertheless, the ultrafast laser welding technique has no equivalent in the semiconductor–metal configuration which would enable applications in photovoltaics, sensors, and, more generally, microelectronics. This lack originates from the strong nonlinear propagation effects in semiconductors leading to a mediocre energy deposition at the interface between both materials. Ultrashort laser pulses are prone to exhibit a filament propagation originating from the competition between the optical Kerr effect and multi-photon ionization leading to defocusing.[13] In materials exhibiting high nonlinear coefficients such as silicon, filaments form at modest pulse energies,[14,15] which has two

Dr. M. Chambonneau, Dr. Q. Li, M. Blothe, Prof. S. Nolte
Institute of Applied Physics
Abbe Center of Photonics
Friedrich Schiller University Jena
Albert-Einstein-Straße 15, Jena 07745, Germany
E-mail: maxime.chambonneau@uni-jena.de;
maxime.chambonneau@hotmail.fr
Dr. V. Y. Fedorov, Prof. S. Tzortzakis
Science Program Texas A&M University at Qatar
Doha P.O. Box 23874, Qatar

Dr. V. Y. Fedorov
P. N. Lebedev Physical Institute of the Russian Academy of Sciences
53 Leninskiy Prospekt Moscow 119991, Russia
K. Schaarschmidt, M. Lorenz
Leibniz Institute of Photonic Technology
Albert-Einstein-Straße 9
Jena 07745, Germany
Prof. S. Tzortzakis
Institute of Electronic Structure and Laser (IESL)
Foundation for Research and Technology–Hellas (FORTH)
P.O. Box 1527 Heraklion GR-71110, Greece
Prof. S. Tzortzakis
Materials Science and Technology Department
University of Crete
Heraklion 71003, Greece
Prof. S. Nolte
Fraunhofer Institute for Applied Optics and Precision Engineering IOF
Center of Excellence in Photonics
Albert-Einstein-Straße 7, Jena 07745, Germany

**ADVANCED
SCIENCE NEWS**

www.advancedsciencenews.com

LASER
& PHOTONICS
REVIEWS

www.lpr-journal.org

major consequences. First, the significant losses induced by two-photon absorption and the filament formation limit the maximum intensity reachable inside silicon at a level below its modification threshold.[16–18] This intensity clamping phenomenon thus implies that increasing the input pulse energy is not a well-adapted strategy for modifying permanently silicon through a plane entrance surface.[19] The second consequence is the nonlinear focal shift at increasing input power, away from the desired location.[15,17–21] Taken together, these processes lead to a drastic depletion of the light at the exit surface of silicon to levels insufficient for laser welding applications. To date, the most efficient and reliable method for circumventing these nonlinear effects is to employ nanosecond laser pulses. While this solution is adequate for in-volume functionalization silicon,[22,23] the thermo-structural processes inherent to this long pulse duration regime are inappropriate for reaching a sufficient degree of control of the energy deposition during laser welding.[24] The picosecond regime thus naturally appears to be an excellent compromise for reducing both the nonlinear propagation and the thermo-mechanical effects in laser welding applications. However, no characterization of the nonlinear propagation in silicon has been carried out in this regime so far.

In this article, we demonstrate the absence of a physical limit for semiconductor–metal ultrafast laser welding, and we illustrate this with silicon and copper. We experimentally study the formation of filaments induced in silicon by picosecond pulses employing nonlinear propagation imaging to determine the nonlinear focal shift. Precompensating for this shift allows us to maximize the light intensity at the interface between silicon and copper leading to effective welding of the materials. Shear joining strength measurements reveal that our proposed method yields 2.2 MPa between the samples, thus holding a high potential for applications. Material analyses with electron microscopy and Raman spectroscopy highlight the wide variety of involved physical mechanisms.

2. Experimental Arrangement

The experimental arrangement for welding silicon samples on copper is detailed in Sections S1.1 and S1.2, Supporting Information. Briefly, it relies on 9.8-ps duration pulses [full width at half-maximum, (FWHM)] emitted at 100-kHz repetition rate by an erbium-doped fiber laser at 1555-nm wavelength. As previously mentioned, the choice of using this pulse duration rather than extremely short pulses (on the order of 100 fs) is mainly motivated by the diminution of the nonlinear propagation effects. Moreover, Penilla et al. have shown that 1-ps pulses lead to more efficient welding than 230-fs pulses.[12] Therefore, employing picosecond pulses should lead to significant—but not excessive—thermal effects, which are a prerequisite for laser welding. The Gaussian beam is focused through silicon at the interface with copper by means of an objective lens of numerical aperture NA = 0.26 mounted on a translation stage allowing its displacement along the optical axis z. At the focus, the beam diameter at $1/e^2$ is $2w_0 = 5.4$ μm. The two samples are stacked together without optical contact or any fixture, and moved together in the xy plane (perpendicular to the laser propagation axis z). The welding pattern is based on a raster scan procedure with a 10-μm distance between the lines and a total scanned area of 4.5×4.5 mm^2. The
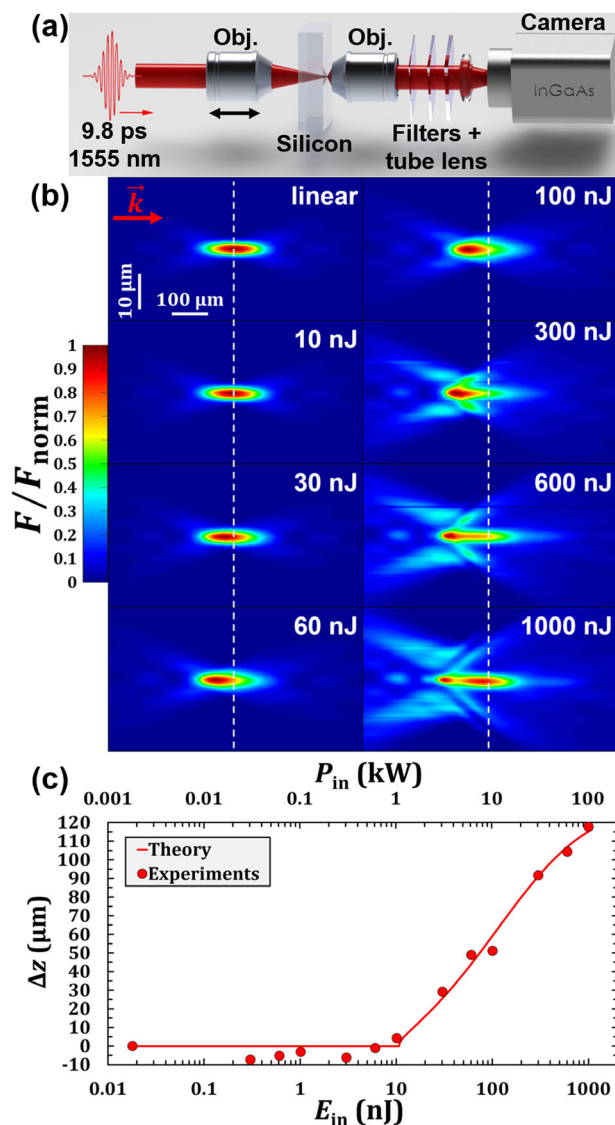

Figure 1. a) Schematic of the nonlinear propagation imaging system. b) Normalized fluence distributions (F/F_{norm}) in bulk silicon for different input pulse energies E_{in}. The white dashed lines indicate the geometrical focus in the linear case ($E_{in} = 18$ pJ). The vector $\vec{k}$ shows the direction of the laser propagation. c) Comparison between calculations of the theoretical focal shift Δz for various E_{in} values (corresponding to the input peak power in air P_{in}) according to Equation (1), and experimental values from (b).

shear joining strength between the two samples is measured after the welding experiments by means of an indenter (see Section S1.3, Supporting Information). The nonlinear propagation inside silicon is characterized prior to the welding with the set-up shown in **Figure 1**a. The corresponding experimental procedure relies on the imaging of the exit surface of the silicon sample thanks to a collecting objective lens (NA = 0.85), and an InGaAs array (see Section S1.4, Supporting Information). The focusing objective lens is moved along z and an image is recorded after each movement. The fluence distribution is reconstructed for various input pulse energies E_{in} (measured in air at the focus) by stacking

ADVANCED
SCIENCE NEWS

www.advancedsciencenews.com
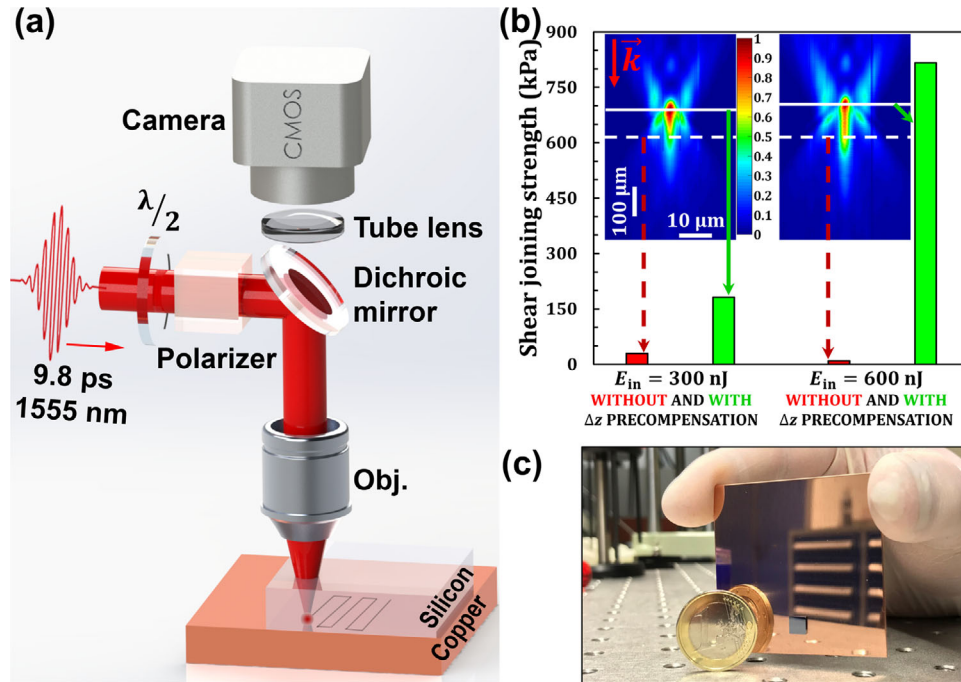
LASER &
PHOTONICS
REVIEWS

www.lpr-journal.org

Figure 2. a) Schematic of the ultrafast laser welding set-up. b) Laser-induced shear joining strength between silicon and copper for an input pulse energy E_{in} = 300 nJ and 600 nJ without (in red) and with (in green) precompensation of the nonlinear focal shift Δz. The insets are the corresponding fluence distributions extracted from Figure 1b. The vector $\vec{k}$ shows the direction of the laser propagation. The solid and dashed white lines indicate the position of the interface between the two samples in each configuration. c) Photograph of an ultrafast-laser-welded 5×5-mm^2 size crystalline silicon sample on copper.

together the cross-sections of the images along one transversal axis. The non-destructive aspect of the imaging procedure is ensured by sample inspection under white light illumination.

3. Results and Discussion

Typical normalized fluence distributions (F/F_{norm}) in silicon are displayed in Figure 1b. Three different regimes are exhibited. The first one is the linear propagation regime (input pulse energy $E_{in} \leq 10$ nJ), in good agreement with point spread function analyses (see Section S2, Supporting Information). This enables us to determine the position of the geometrical focus z_g (white dashed lines), positioned at the exit surface of the silicon sample. In the second regime, for 10 nJ < $E_{in} \leq 100$ nJ, the position of the maximum intensity z_{max} is unambiguously shifted upstream the incoming laser with respect to the position z_g. This focal shift toward the prefocal region in accordance with observations in the femtosecond regime[17–21] highlights the existence of nonlinear propagation effects. Nevertheless, the resulting focal zone is still comparable in its extension to the linear case, while the shape of the fluence distribution deviates from the linear one with increasing pulse energies. Noteworthy, analogous focal shifts were observed in glass under femtosecond laser exposure at a high repetition rate (> 1 MHz).[25] However, these shifts originate from heat accumulation effects in the dielectric exhibiting low heat conductivity. In contrast, in our configuration where laser pulses are focused inside silicon at a much lower repetition rate, no heat accumulation is expected. Finally, in the third regime where $E_{in} \geq 300$ nJ, more pronounced filamentation defocusing and re-

focusing dynamics are observed. The shape of the fluence distribution in this regime is no longer comparable to the linear case. The evolution of the nonlinear focal shift $\Delta z = z_{max} - z_g$ is displayed in Figure 1c as a function of E_{in} and the corresponding peak power in air P_{in}. For $E_{in} \leq 10$ nJ, there is no significant nonlinear focal shift Δz. However, for $E_{in} \geq 30$ nJ, Δz increases up to 117 μm and scales logarithmically with E_{in}, so that z_{max} is not located anymore at the exit surface of the sample, but it is in the bulk of silicon.

One can consider that the nonlinear focal shift Δz experimentally determined in Figure 1 results from two mechanisms which are i) the linear focusing caused by the focusing objective lens (with a propagation distance from the entrance surface of the silicon sample to the geometrical focus $f^* = 1$ mm, corresponding to the sample thickness), and ii) the optical Kerr effect (considered as a distributed lens with an effective focal distance z_{nl}). This shift thus reads

$$\Delta z = f^* - \left(1/f^* + 1/z_{nl}\right)^{-1} \tag{1}$$

To calculate the value of z_{nl}, we apply a Marburger-type formula[26] where we take into account that the peak laser power is reduced due to two-photon absorption (see the details in Section S3.1, Supporting Information). The resulting theoretical model has two free parameters: the critical power for Kerr self-focusing P_{cr}, and the effective two-photon absorption coefficient β_2^* (defined for power rather than intensity, see Section S3.1, Supporting Information). Using Equation (1) as the fitting function we applied nonlinear curve fitting to the experimental data and

ADVANCED
SCIENCE NEWS
www.advancedsciencenews.com

LASER
& PHOTONICS
REVIEWS

www.lpr-journal.org

found $P_{cr} = 0.65$ kW and $\beta_2^* = 0.112$ W^{-1} m^{-1} to be the optimal values. Figure 1c shows that the obtained fitting curve is in excellent agreement with the experimental data, which allows us to conclude that the major physical mechanisms responsible for the nonlinear shift are described correctly. Thus, using our semi-analytical model we can accurately predict the position of the maximum intensity. Ultimately, our theoretical approach was benchmarked by additional nonlinear propagation measurements of 860-fs pulses, also in good agreement with the theoretical predictions of Equation (1) (see Section S3.2, Supporting Information).

For significant nonlinear focal shift values Δz, any attempt of ultrashort laser welding between silicon and another material with an interface located at the geometrical focus is doomed to failure. Therefore, we devise a welding optimization method consisting of the determination and the precompensation of Δz by moving the focusing objective lens downstream the laser flux for welding. In order to demonstrate the efficiency of this procedure, laser welding of silicon and copper has been endeavored with and without it by means of the experimental arrangement shown in **Figure 2**a. Typical results are displayed in terms of shear joining strength in Figure 2b for two input pulse energies, with and without precompensation of Δz. For both energies, a shear joining strength <30 kPa is measured when the geometrical focus is simply positioned at the interface between the samples. The two samples are easily separable in this case, and thus not suitable for applications. In stark contrast, a precompensation of the position of the focusing objective lens by the predetermined nonlinear focal shift Δz yields shear joining strengths of 182 kPa and 817 kPa for $E_{in} = 300$ and 600 nJ, respectively. These results demonstrate the considerable advantage to account for the nonlinear propagation effects for semiconductor–metal ultrafast laser welding as illustrated in Figure 2c.

As displayed in **Figure 3**a, not only the nonlinear focal shift depends on E_{in}, but also the maximum fluence F_{max} and the energy reaching the silicon-copper interface E_{Si-Cu}. When the nonlinear propagation threshold (purple line) is crossed, precompensating the nonlinear focal shift Δz is required for optimizing the maximum fluence F_{max} at the interface. However, this optimization is limited by the intensity clamping phenomenon saturating the maximum fluence in silicon.[17–19] In contrast, the energy reaching the silicon-copper interface E_{Si-Cu} increases with E_{in} without any saturation. One must emphasize that, again, the precompensation of Δz is crucial for enhancing E_{Si-Cu}, especially for high E_{in} values. This is ascribable to the strong prefocal absorption drastically depleting E_{Si-Cu} if no precorrection of Δz is made. From the data in Figure 3a, one can conclude that the precompensation of the nonlinear focal shift considerably enhances both the maximum fluence, as well as the energy reaching the silicon-copper interface during welding. In order to further explore the potential of our proposed Δz-precompensation method for semiconductor–metal ultrafast laser welding, experiments have been carried out for various input pulse energies E_{in}. As shown in Figure 3b, overall, the higher E_{in}, the more efficient the ultrashort laser welding. Precompensating the nonlinear focal shift yields shear joining strengths up to 2.2 MPa. The strength values displayed in Figure 3b are comparable to those obtained with the laser welding technique in other material configurations[7–12] as well as with adhesive bonding. Insignificant strengths (≤ 50 kPa)
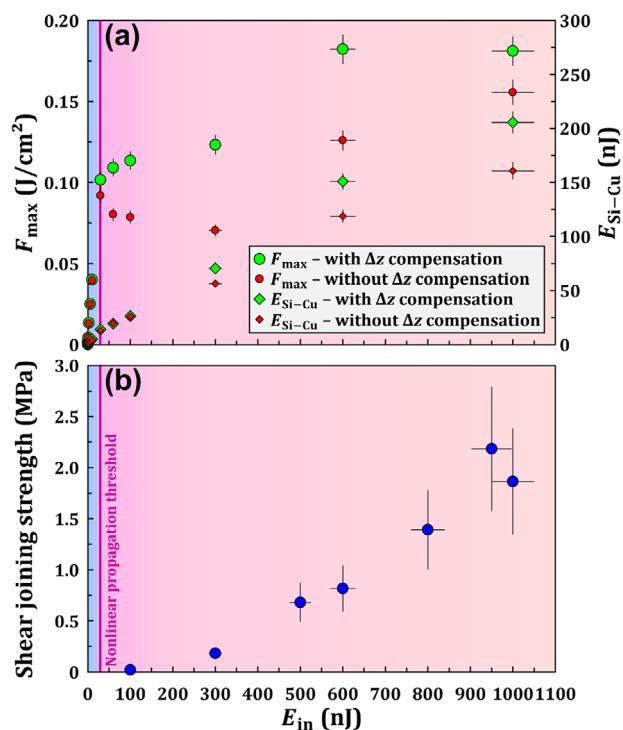

Figure 3. a) Evolution of the maximum fluence F_{max}, and the energy reaching the silicon–copper interface E_{Si-Cu} with and without precompensation of the nonlinear focal shift Δz, as well as b) the shear joining strength between silicon and copper induced by Δz-precompensated ultrafast laser welding as a function of the input pulse energy E_{in}. The blue and red domains delimited by the nonlinear propagation threshold (purple line) correspond to the linear and the nonlinear propagation regimes, respectively. The error bars on the energy and the fluence values stand for the accuracy of the employed power meter (5%), and those on the shear strength values stand for the repeatability (27.9%, see Section S1.3, Supporting Information).

have been measured for $E_{in} \leq 100$ nJ since the modification threshold of copper is not reached at these input pulse energies, as confirmed with scanning electron microscopy (SEM). Interestingly, this result indicates that semiconductor–metal ultrafast laser welding is solely achievable in the nonlinear propagation regime, highlighting the importance of the Δz-precompensation.

Ultimately, material analyses of the welds have been carried out on both the silicon and the copper samples. Typical results after sample separation subsequent to ultrafast laser welding at $E_{in} = 950$ nJ are shown in **Figure 4**. The SEM image of the copper sample in Figure 4a exhibits dark (1) and bright features (2) originating from different charging rates of the observed areas. Raman spectra have been obtained on both of these feature types in Figure 4b. The dark features (1) show a similar Raman signal as non-irradiated copper, suggesting the absence of silicon in these zones. In contrast, the Raman spectrum in the bright features (2) exhibits a peak centered at 507 cm^{-1}, revealing the presence of silicon in these zones. The 13-cm^{-1} difference between this peak and the Raman signature peak of mono-crystalline silicon (around 520 cm^{-1}) may originate from strong local strain fields inside the material.[27] Moreover, the enhanced signal at 100–200 cm^{-1} as well as at 430–500 cm^{-1} suggests that the features (2)

ADVANCED
SCIENCE NEWS

www.advancedsciencenews.com
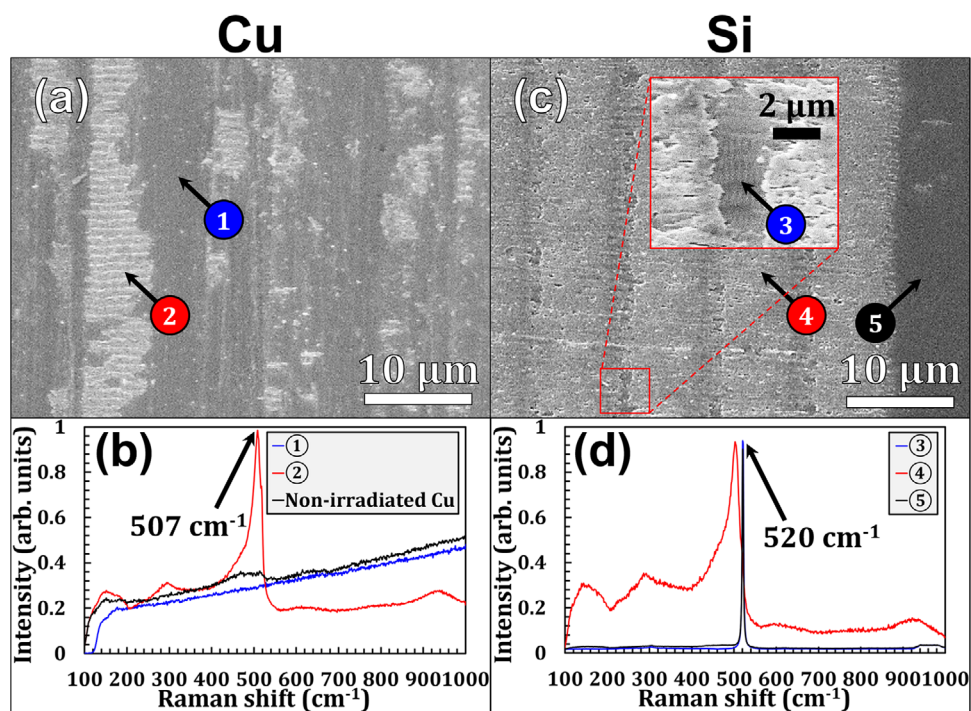
LASER
& PHOTONICS
REVIEWS

www.lpr-journal.org

Figure 4. Material analyses of laser welds (E_{in} = 950 nJ). SEM images of a) the copper and c) the silicon sample. The inset in (c) shows typical ripples between lines. b,d) Raman spectroscopy measurements in the areas indicated in (a) and (c), respectively.

result from partially amorphous silicon.[28] One must emphasize that these silicon parts are still bonded on copper even after the sample separation, which may originate from the creation of covalent bonds, again demonstrating the efficiency of our proposed welding method. Concerning the silicon sample, the SEM image in Figure 4c exhibits lines (4) of molten material that are brighter than the non-irradiated zone (5). These lines separated by 10 µm obviously correspond to the ones scanned by the laser with the same line pitch. The molten aspect of these lines sheds light on the high-temperature phenomena provoked by the laser. Interestingly, the zones (3) between the lines exhibit nanostructures (of 280-nm period) as shown in the inset of Figure 4c. The morphology of these nanostructures is analogous to the one of ripples [also known as laser-induced periodic surface structures (LIPSS)].[29] While LIPSS are usually produced in different conditions (i.e., only one material irradiated at the entrance surface), they may highlight the role of surface plasmons during the welding procedure.[30] Ultimately, Raman spectra have been measured in different zones of the silicon sample. As shown in Figure 4d, the zones (3) exhibiting ripples show similar features as the non-irradiated mono-crystalline silicon (5). By contrast, the irradiated zones (4) exhibit the aforementioned characteristic features of amorphous silicon. This indicates a partial laser-induced amorphization of silicon.

It is important to highlight that, while no bulk or surface damage is produced in silicon during the nonlinear propagation imaging procedure, the presence of an interface with a metal provokes a modification of the exit surface as shown in Figure 4c. This drastic change in the material behavior also observed in femtosecond backside ablation of gold film on a silicon substrate[31]

can be attributed to two mechanisms. First, the copper interface involves a strong reflection of the laser flux which has not been absorbed during the nonlinear propagation. This reflection thus leads to an increase in the energy deposited at the exit surface of silicon. In addition, the residual air gap between the samples could act as a Fabry–Perot cavity, thus enhancing locally the laser intensity. Second, the metal exhibits free electrons that are able to linearly absorb the laser flux by inverse Bremsstrahlung, which is particularly efficient for infrared wavelengths such as the one inevitably employed for reaching the silicon-copper interface. This leads to a significant temperature increase at the interface.

4. Conclusion

To summarize, silicon–copper laser welding was demonstrated using picosecond infrared laser pulses. These results were possible thanks to the determination and the precompensation of the nonlinear focal shift in silicon inherent to the ultrashort infrared pulses. The precompensation of this shift enabled us to obtain shear joining strength up to 2.2 MPa—thus suitable for applications in various fields where semiconductors and metals are the backbone materials of complex microelectronic devices. Material analyses shed light on the physical mechanisms involved during the welding, which might include silicon amorphization, covalent bond creation, and surface plasmon excitation. Given that strong nonlinear propagation effects exist in most narrow-gap semiconductors, the proposed ultrafast laser welding technique relying on the precompensation of the nonlinear focal shift has the potential to be applied in numerous

semiconductor–metal configurations. Moreover, we anticipate that this technique is also applicable in several semiconductor–semiconductor configurations where at least the first material is transparent to the laser wavelength.

5. Experimental Section

Samples: During both the nonlinear propagation and the ultrafast welding experiments, microelectronic-grade silicon (Si) samples have been employed (Siegert Wafer, Czochralski growth, undoped, double-side polished, 1-mm thickness, <100>-oriented, >200-Ω·cm resistivity). The 50.8 ± 0.3-mm diameter wafer was cut into individual 5×5-mm^2 samples and their edges were subsequently polished. The copper (Cu) samples on which the silicon samples were stacked up have been employed during the ultrafast laser welding experiments (Goodfellow, double-side polished, 0.5-mm thickness, half hard tempered, 99.95% purity).

Laser System: The same laser source was employed for both the nonlinear propagation imaging and the ultrafast welding experiments. This source is an erbium-doped fiber laser (Raydiance Inc., Smart Light 50). The average power stability of the laser was <1%. The laser center wavelength was 1555 nm. The repetition rate was set to 100 kHz. The pulse duration was adjustable between 0.86 and 9.8 ps. Most of the results of this study were obtained with 9.8-ps duration pulses in order to decrease the nonlinear effects in silicon. The output spatial profile was Gaussian and its diameter at $1/e^2$ was adjusted to 10.6 mm by means of a Galilean telescope before focusing with an objective lens of numerical aperture 0.26 (Mitutoyo, M Plan Apo NIR 10×).

Nonlinear Propagation Imaging: In order to access the 3D fluence distribution at the silicon-copper interface, nonlinear propagation imaging was carried out in silicon. The rear surface of the silicon sample was imaged with a customized infrared microscope composed of a high numerical aperture (NA = 0.85) objective lens (Olympus, LCPLN100XIR), a tube lens (Thorlabs, TTL200-S8), and an InGaAs camera (Xenics, Bobcat 320). The high magnification (100×) associated with this microscope enables to reach an image size of 58.40×46.72 μm^2. The incoming laser beam was focused with the same objective lens as the one employed in the subsequent ultrafast welding experiments, in the opposite direction of this microscope. By moving the focusing objective lens along the optical axis with computer-controlled steps and by acquiring images after each step, the 3D fluence distribution in silicon for various input pulse energies was reconstructed—thus allowing us to determine the nonlinear focal shift.

Modeling the Linear Propagation: The calculations of the theoretical 3D fluence distribution during linear propagation in silicon have been carried out by means of a dedicated full-vectorial model relying on point spread function analysis. The simulations consisted of calculations of the volumetric electric field distribution in the focal region of the objective lens based on the vector diffraction theory and the chirp z-transform (CZT) algorithms. A comparison between the theoretical calculations and the linear propagation experiments yielded an excellent agreement, thus validating the theoretical approach.

Modeling the Nonlinear Focal Shift: The calculations of the theoretical nonlinear focal shift relied on a combination of the linear focusing with the objective lens and the contribution of the optical Kerr effect. This latter was determined thanks to a Marburger-type formula, where losses provoked by two-photon absorption were accounted for. The theoretical approach was benchmarked with additional nonlinear propagation imaging measurements with 860-fs duration pulses.

Ultrafast Laser Welding: During the semiconductor–metal ultrafast laser welding, the silicon and the copper samples were stacked up on nanopositioning stages (Aerotech, ANT130-160-XY) allowing accurate displacements in the xy plane perpendicular to the optical axis z. The laser pulses were focused with the same objective lens as the one employed during nonlinear propagation imaging. The displacement of this objective lens along z is ensured by another nanopositioning stage (Aerotech, ANT130-060-L). Damage scans on the entrance surface enabled to obtain the relative position of the geometrical focus and the sample as well as its tilt. The geometrical focus was then positioned at the silicon-copper interface by moving the objective lens toward the samples by the ratio between the thickness of the silicon sample and the refractive index of silicon. In the nonlinear propagation regime, an additional precompensation of the nonlinear focal shift Δz was applied according to the Δz values obtained with nonlinear propagation imaging. Once the position of the focus along z was selected, the samples were moved together in the xy plane following a raster scan (1-mm s^{-1} scanning speed, 10-μm line pitch, 4.5×4.5-mm^2 total area).

Analyses of the Welds: The welds have been first characterized in terms of shear joining strength. An indenter (cylindrical shape, 7.4-mm diameter) was employed for separating the samples, while the force for which the samples were disjoint was recorded by a force gauge (RS PRO, 111-3690). The shear joining strength was obtained by calculating the ratio between this force and the welded area. The silicon and the copper sample surfaces were characterized under SEM (LEO, 435VP) and Raman spectroscopy (Renishaw, inVia) at 532-nm wavelength employing an objective lens of numerical aperture NA = 0.85.

Supporting Information

Supporting Information is available from the Wiley Online Library or from the author.

Conflict of Interest

The authors declare no conflict of interest.

[1] A. Rousse, C. Rischel, S. Fourmaux, I. Uschmann, S. Sebban, G. Grillon, Ph. Balcou, E. Förster, J. P. Geindre, P. Audebert, J. C. Gauthier, D. Hulin, *Nature* **2001**, *410*, 65.

[2] S. K. Sundaram, E. Mazur, *Nat. Mat.* **2002**, *1*, 217.

[3] K. Sokolowski-Tinten, C. Blome, J. Blums, A. Cavalleri, C. Dietrich, A. Tarasevitch, I. Uschmann, E. Förster, M. Kammler, M. Horn-von-Hoegen, D. von der Linde, *Nature* **2003**, *422*, 287.

[4] R. R. Gattass, E. Mazur, *Nat. Photon.* **2008**, *2*, 219.

[5] C. Kerse, H. Kalaycıoğlu, P. Elahi, B. Çetin, D. K. Kesim, Ö. Akçaalan, S. Yavaş, M. D. Aşık, B. Öktem, H. Hoogland, R. Holzwarth, F. Ö. Ilday, *Nature* **2016**, *537*, 84.

ADVANCED
SCIENCE NEWS

www.advancedsciencenews.com

LASER
& PHOTONICS
REVIEWS

www.lpr-journal.org

[6] M. F. Yanik, H. Cinar, H. N. Cinar, A. D. Chisholm, Y. Jin, A. Ben-Yakar, *Nature* **2004**, *432*, 822.

[7] G. Zhang, G. Cheng, *Appl. Opt.* **2015**, *54*, 8957.

[8] G. Zhang, R. Stoian, W. Zhao, G. Cheng, *Opt. Express* **2018**, *26*, 917.

[9] S. Richter, F. Zimmermann, A. Tünnermann, S. Nolte, *Opt. Laser Technol.* **2016**, *83*, 59.

[10] K. Cvecek, S. Dehmel, I. Miyamoto, M. Schmidt, *Int. J. Extrem. Manuf.* **2019**, *1*, 042001.

[11] I. Mingareev, F. Weirauch, A. Olowinsky, L. Shah, P. Kadwani, M. Richardson, *Opt. Laser Technol.* **2012**, *44*, 2095.

[12] E. H. Penilla, L. F. Devia-Cruz, A. T. Wieg, P. Martinez-Torres, N. Cuando-Espitia, P. Sellappan, Y. Kodera, G. Aguilar, J. E. Garay, *Science* **2019**, *365*, 803.

[13] A. Couairon, A. Mysyrowicz, *Phys. Rep.* **2007**, *441*, 47.

[14] V. Yu. Fedorov, M. Chanal, D. Grojo, S. Tzortzakis, *Phys. Rev. Lett.* **2016**, *117*, 043902.

[15] M. Chambonneau, L. Lavoute, D. Gaponov, V. Y. Fedorov, A. Hideur, S. Février, S. Tzortzakis, O. Utéza, D. Grojo, *Phys. Rev. Appl.* **2019**, *12*, 024009.

[16] A. Mouskeftaras, A. V. Rode, R. Clady, M. Sentis, O. Utéza, D. Grojo, *Appl. Phys. Lett.* **2014**, *105*, 191103.

[17] E. V. Zavedeev, V. V. Kononenko, V. I. Konov, *Laser Phys.* **2016**, *26*, 016101.

[18] E. I. Mareev, K. V. Lvov, B. V. Rumiantsev, E. A. Migal, I. D. Novikov, S. Y. Stremoukhov, F. V. Potemkin, *Laser Phys. Lett.* **2020**, *17*, 015402.

[19] M. Chanal, V. Y. Fedorov, M. Chambonneau, R. Clady, S. Tzortzakis, D. Grojo, *Nat. Commun.* **2017**, *8*, 773.

[20] V. V. Kononenko, V. V. Konov, E. M. Dianov, *Opt. Lett.* **2012**, *37*, 3369.

[21] V. V. Kononenko, E. V. Zavedeev, V. M. Gololobov, *Appl. Phys. A* **2016**, *122*, 293.

[22] M. Chambonneau, Q. Li, M. Chanal, N. Sanner, D. Grojo, *Opt. Lett.* **2016**, *41*, 4875.

[23] O. Tokel, A. Turnalı, G. Makey, P. Elahi, T. Çolakoğlu, E. Ergeçen, Ö. Yavuz, R. Hübner, M. Z. Borra, I. Pavlov, A. Bek, R. Turan, D. K. Kesim, S. Tozburun, S. Ilday, F. Ö. Ilday, *Nat. Photon.* **2017**, *11*, 639.

[24] Y. Ozeki, T. Inoue, T. Tamaki, H. Yamaguchi, S. Onda, W. Watanabe, T. Sano, S. Nishiuchi, A. Hirose, K. Itoh, *Appl. Phys. Express* **2008**, *1*, 0826011.

[25] I. Miyamoto, Y. Okamoto, A. Hansen, J. Vihinen, T. Amberla, J. Kangastupa, *Opt. Express* **2016**, *24*, 25718.

[26] J. H. Marburger, *Prog. Quant. Electron.* **1975**, *4*, 35.

[27] T. A. Langdo, M. T. Currie, A. Lochtefeld, R. Hammond, J. A. Carlin, M. Erdtmann, G. Braithwaite, V. K. Yang, C. J. Vineis, H. Badawi, M. T. Bulsara, *Appl. Phys. Lett.* **2003**, *82*, 4256.

[28] P. A. Temple, C. E. Hathaway, *Phys. Rev. B* **1973**, *7*, 3685.

[29] G. D. Tsibidis, M. Barberoglou, P. A. Loukakos, E. Stratakis, C. Fotakis, *Phys. Rev. B* **2012**, *86*, 115316.

[30] E. Petrakakis, G. D. Tsibidis, E. Stratakis, *Phys. Rev. B* **2019**, *99*, 195201.

[31] S. Lei, D. Grojo, J. Ma, X. Yu, H. Wu, *Procedia Manuf.* **2016**, *5*, 594.